



Phonon-assisted optical absorption of SiC polytypes from first principlesXiao Zhang  and Emmanouil Kioupakis ^{*}*Department of Materials Science and Engineering, The University of Michigan, Ann Arbor, Michigan 48109, USA*

(Received 12 January 2023; accepted 20 March 2023; published 30 March 2023)

Silicon carbide (SiC) is an indirect-gap semiconductor material widely used in electronic and optoelectronic applications. While experimental measurements of the phonon-assisted absorption coefficient of SiC across its indirect gap have existed for more than 50 years, theoretical investigations of phonon-assisted absorption have been hampered by their excessive computational cost. In this work, we calculate the phonon-assisted temperature-dependent optical absorption spectra of the commonly occurring SiC polytypes (3C, 2H, 4H, 6H, and 15R), using first-principles approaches based on density functional theory and related techniques. We show that our results agree with experimentally determined absorption coefficients in the spectral region between the direct and indirect band gaps. The temperature dependence of the spectra can be well predicted with taking the temperature dependence of the band gaps into account. Lastly, we compare the spectra obtained with second-order perturbation theory to those determined by the special displacement method and we show that the full consideration of the electronic energy renormalization due to temperature is important to further improve the prediction of the phonon-assisted absorption in SiC. Our insights can be applied to predict the optical spectra of the less common SiC polytypes and other indirect-gap semiconductors in general.

DOI: [10.1103/PhysRevB.107.115207](https://doi.org/10.1103/PhysRevB.107.115207)**I. INTRODUCTION**

Silicon carbide (SiC) is an indirect gap semiconductor material that has been well established and widely used in many electronic and optoelectronic devices. It has a variety of structural polytypes, including cubic 3C, hexagonal 2H, 4H, 6H, and several rhombohedral structures (9R, 15R, etc.) [1–3], that enable a broad range of applications. Its 6H polytype is one of the first to be used to create blue light emitting diodes (LEDs) that enabled full color LEDs [4], though the indirect band gap limits the efficiency. Absorbing short-wavelength light much more efficiently, the material is also used as UV-sensitive diodes in flame sensors [4–6]. More recently, SiC is widely used as substrate material for applications such as extreme condition transistors [7–9], tunable photodetecting devices [10], and advanced UV detectors [11–13]. Recent developments in crystal growth also allowed novel structures such as thin films, nanoparticles, heterostructures, etc., for more advanced applications [14–17]. Due to its early discovery as well as the wide applications and interest, it is now one of the most well studied semiconductor materials from both an experimental and a theoretical point of view.

Understanding the similarities and differences between the structural polytypes is crucial for practical applications. The most common SiC polytypes for application purposes are the cubic structure (3C) and two hexagonal structures with different stackings (4H and 6H). It has been shown both by experimental and theoretical studies [18] that, at low temperatures, SiC tends to form the cubic 3C structure while, at higher temperatures, 4H and 6H become the more energetically favorable structures. In addition to 4H and 6H, the 2H structure

of SiC has also been observed, although rarely due to being energetically less favorable. Due to its rare occurrence, the optoelectronic properties of the 2H polytype have not been studied thoroughly from either a theoretical or an experimental perspective, and previous studies are typically limited to only structural properties and basic electronic properties such as the band gap. The rhombohedral structure of SiC is less commonly seen but can also be grown on various temperatures and substrates [19–21] and has been shown to demonstrate great potential in MOSFET applications [19,21]. Overall, the natural occurrence of these different polytypes makes it an important task to study them consistently from a first-principles perspective to understand the properties of the material better and potentially discover new opportunities for applications.

Despite being well studied for many polytypes, the indirect optical properties of SiC, which are important considering its applications in optoelectronic devices, have never been thoroughly studied with first principles techniques. Experimental characterization of its indirect gap and optical absorption in the spectral region between the indirect and direct band gaps has existed ever since the 1960s [22,23]. There has also been a considerable number of theoretical calculations of optical properties for both bulk SiC and nanostructures, however, always focusing on direct transitions [24–30]. The commonly used theoretical spectroscopy approaches based on the density functional theory lack descriptions of electron-phonon interactions. As a result, momentum transfer is neglected in considering optical absorption and such approaches are only able to consider direct transitions. Yet indirect optical absorption plays an important role in the application of SiC as the difference between the direct gap and the indirect gap can range from about 1 eV up to more than 3 eV, depending on the polytype [2]. As an example, although SiC was one of the first LED materials for blue light mission, it can only emit

^{*}kioup@umich.edu

visible light via phonon-assisted transitions across its indirect band gap. Although being considerably weaker compared to direct transitions, the phonon-assisted contribution enabled its application in optoelectronic devices. Therefore, the lack of theoretical studies on the indirect optical properties of SiC significantly limits our ability to understand the material and its further potential applications in optoelectronic devices.

There are numerous computational challenges on evaluating phonon-assisted optical properties from a theoretical perspective and tools to model them have only emerged in recent years. One significant challenge is the necessity of dense sampling of the electronic states in the first Brillouin zone, due to the broad energy range of photon frequencies, combined with the large number of processes needed to be considered in second-order transition. While the latter makes the problem more complicated by nature, the task of studying electron-phonon properties with dense electronic and phonon Brillouin-zone sampling grids can be overcome by the approach of maximally localized Wannier function interpolation [31]. The Wannier interpolation starts from a coarse grid of electronic states, finds a set of maximally localized Wannier functions to represent the electronic wave functions in the real space, and utilizes such a set of Wannier functions to construct the electronic wave functions in a dense grid of the electronic states. It has been shown that Wannier interpolation can result in accurate interpolations for both the electronic structures and electron-phonon coupling matrix elements in a broad range of materials [32]. It thus becomes feasible to calculate electron-phonon properties on a coarse grid with reasonable computational cost, then utilize Wannier interpolation to determine the phonon-assisted optical absorption spectra with adequate spectral resolution.

In this work, we perform first-principles calculations to understand the phonon-assisted optical absorption spectra for common SiC polytypes (3C, 2H, 4H, 6H, and 15R). As in experimental measurements, the absorption coefficients are mostly measured along the c axis ($E \perp c$); thus in our work we report and compare the calculated absorption coefficient for the ordinary direction as well. By combining standard first-principles approaches (DFT, many-body perturbation theory) for electronic structure and direct optical properties along with Wannier interpolation for electron-phonon coupling, we show that our calculated indirect optical spectra are in good agreement with available experimental measurements. We further predict the phonon-assisted spectra for polytypes for which experimental data are lacking. Our approach well predicts the temperature dependence of the indirect optical spectra, which can benefit the applications of SiC in extreme conditions. Further, by comparing to the special displacement method (SDM) [33–35], we show that, to further improve the predictions of indirect optical properties as a function of temperature, both the effects of temperatures on the optical spectra due to changes in phonon occupation factors and the effects of temperatures on the electronic energy renormalization are important.

II. COMPUTATIONAL APPROACH

To calculate the structural, electronic, and optical properties of the SiC polytypes, we performed first-principles

calculations based on density functional theory. The calculation is carried out with the QUANTUM ESPRESSO [36,37] package using the Perdew-Burke-Ernzerhof (PBE) [38] approximation for the exchange-correlation functional and the SG15 optimized norm-conserving Vanderbilt (ONCV) pseudopotentials [39,40]. The wave functions are expanded into plane waves up to an energy cutoff of 60 Ry. Structural relaxation is done for all polytypes until all the components of the forces on the atoms are smaller than 10^{-5} Ry/bohr. Converged ground-state calculations for each polytype were performed with Brillouin-zone (BZ) sampling grids of $8 \times 8 \times 8$ for 3C, $12 \times 12 \times 8$ for 2H, $12 \times 12 \times 4$ for 4H, $10 \times 10 \times 2$ for 6H, and $8 \times 8 \times 8$ for 15R. In all cases, the grid is shifted by half a grid spacing to improve convergence.

To correct the underestimation of the band gap by PBE, we calculated quasiparticle energies with the one-shot GW method (G_0W_0) using the BERKELEYGW package [41,42]. The static dielectric matrix is evaluated in the random phase approximation and extended to finite frequency with the generalized plasmon-pole model by Hybertsen and Louie [41]. The static remainder approach is used to reduce the number of empty orbitals required [43]. The GW calculations are performed with BZ-sampling points grids of $6 \times 6 \times 6$ for 3C, $6 \times 6 \times 4$ for 2H, $6 \times 6 \times 3$ for 4H, and $6 \times 6 \times 2$ and $6 \times 6 \times 6$ for 15R. For all polytypes, the quasiparticle energies were interpolated with the maximally localized Wannier function method [31] to obtain accurate quasiparticle band structures as well as velocity and electron-phonon coupling matrix elements for fine BZ sampling grids in subsequent optical property calculations.

Phonon-related properties are calculated with density functional perturbation theory [44] as implemented in QUANTUM ESPRESSO and interpolated to fine BZ-sampling grids with the maximally localized Wannier function method as implemented in the EPW package [45–48]. The coarse phonon BZ-sampling grids used for the different polytypes are $6 \times 6 \times 6$ for 3C, $6 \times 6 \times 4$ for 2H, $6 \times 6 \times 3$ for 4H, $6 \times 6 \times 2$ for 6H, and $6 \times 6 \times 6$ for 15R. We note that the choices of the coarse BZ samplings are made to ensure both accurate Wannier interpolations as well as retain reasonable computational cost. Since SiC is a polar material, the Fröhlich interaction is considered analytically via a long-range term when calculating the electron-phonon matrix elements [47]. The phonon-assisted optical absorption spectra are determined with second-order time-dependent perturbation theory. Phonon-assisted optical absorption processes are second-order processes in which electrons are not only excited vertically in a band-structure diagram through energy transfer by photon absorption, but also horizontally through momentum transfer with the emission or absorption of phonons. The imaginary part of the dielectric function is derived from second-order time-dependent perturbation theory as [32,48,49]

$$\varepsilon_2(\omega) = \frac{8\pi^2 e^2}{\Omega \omega^2} \frac{1}{N_{\mathbf{k}} N_{\mathbf{q}}} \sum_{\nu j \mathbf{k} \mathbf{q}} |\mathbf{e} \cdot [\mathbf{S}_{1,ij\nu}(\mathbf{k}, \mathbf{q}) + \mathbf{S}_{2,ij\nu}(\mathbf{k}, \mathbf{q})]|^2 \times P_{ij}(\mathbf{k}, \mathbf{q}) \delta(\epsilon_{j,\mathbf{k}+\mathbf{q}} - \epsilon_{i,\mathbf{k}} - \hbar\omega \pm \hbar\omega_{\nu\mathbf{q}}), \quad (1)$$

where the upper (lower) sign represents the phonon emission (absorption) process. Ω is the volume of the unit cell. \mathbf{k} and

\mathbf{q} are the electron and phonon wave vectors. $N_{\mathbf{k}}$ and $N_{\mathbf{q}}$ are the number of \mathbf{k} and \mathbf{q} points in the Brillouin zone sampling. i, j label the band indices and ν labels phonon modes. \mathbf{e} represents the polarization of the light. $\epsilon_{j,\mathbf{k}+\mathbf{q}}$ and $\epsilon_{i,\mathbf{k}}$ are the electronic energies of states $(j, \mathbf{k} + \mathbf{q})$ and (i, \mathbf{k}) , respectively. The generalized matrix elements for the two possible scattering processes are described by the terms $\mathbf{S}_{1,ij\nu}(\mathbf{k}, \mathbf{q})$ [i.e., photon absorption from electronic state (i, \mathbf{k}) to intermediate state (m, \mathbf{k}) followed by electron-phonon scattering from (m, \mathbf{k}) to final state $(j, \mathbf{k} + \mathbf{q})$] and $\mathbf{S}_{2,ij\nu}(\mathbf{k}, \mathbf{q})$ [i.e., electron-phonon scattering from (i, \mathbf{k}) to $(m, \mathbf{k} + \mathbf{q})$ followed by photon absorption from $(m, \mathbf{k} + \mathbf{q})$ to final state $(j, \mathbf{k} + \mathbf{q})$]. Mathematically, the two terms are given by [48,49]

$$\mathbf{S}_{1,ij\nu}(\mathbf{k}, \mathbf{q}) = \sum_m \frac{\mathbf{v}_{im}(\mathbf{k})g_{mj,\nu}(\mathbf{k}, \mathbf{q})}{\epsilon_{m,\mathbf{k}} - \epsilon_{i,\mathbf{k}} - \hbar\omega + i\eta} \quad (2)$$

and

$$\mathbf{S}_{2,ij\nu}(\mathbf{k}, \mathbf{q}) = \sum_m \frac{g_{im,\nu}(\mathbf{k}, \mathbf{q})\mathbf{v}_{mj}(\mathbf{k} + \mathbf{q})}{\epsilon_{m,\mathbf{k}+\mathbf{q}} - \epsilon_{i,\mathbf{k}} \pm \hbar\omega_{\nu\mathbf{q}} + i\eta}. \quad (3)$$

In the equations above, $\mathbf{v}_{ij}(\mathbf{k})$ represents the velocity matrix element for the optical transition between bands i and j at \mathbf{k} and $g_{ij,\nu}(\mathbf{k}, \mathbf{q})$ represents the electron-phonon matrix element describing the scattering process from electronic state (i, \mathbf{k}) to electronic state $(j, \mathbf{k} + \mathbf{q})$ through phonon mode $\nu\mathbf{q}$. In addition, the occupation factor $P_{ij}(\mathbf{k}, \mathbf{q})$ in Eq. (1) is given by combining the Bose-Einstein occupation factor of the phonons $n_{\nu\mathbf{q}}$ and the Fermi occupation factor of the electrons $f_{n\mathbf{k}}$. Considering energy conservation, we obtain the occupation factor for the phonon absorption $P_{a,ij}(\mathbf{k}, \mathbf{q})$ and phonon emission $P_{e,ij}(\mathbf{k}, \mathbf{q})$ process as

$$P_{a,ij}(\mathbf{k}, \mathbf{q}) = n_{\nu\mathbf{q}} \times f_{i,\mathbf{k}} \times (1 - f_{j,\mathbf{k}+\mathbf{q}}) - (n_{\nu\mathbf{q}} + 1) \times (1 - f_{i,\mathbf{k}}) \times f_{j,\mathbf{k}+\mathbf{q}} \quad (4)$$

and

$$P_{e,ij}(\mathbf{k}, \mathbf{q}) = (n_{\nu\mathbf{q}} + 1) \times f_{i,\mathbf{k}} \times (1 - f_{j,\mathbf{k}+\mathbf{q}}) - n_{\nu\mathbf{q}} \times (1 - f_{i,\mathbf{k}}) \times f_{j,\mathbf{k}+\mathbf{q}}. \quad (5)$$

In addition, η in Eq. (2) and Eq. (3) is a numerical broadening parameter to prevent singularities induced by zeros in the denominator that occur when direct transitions are allowed. In our work, we focus on the optical spectra between the indirect band gap and the direct band gap that are not affected by η .

Equations (1) to (5) serve as the foundation of calculating phonon-assisted optical properties from first principles utilizing second-order perturbation theory. In this work, we calculated $\epsilon_2(\omega)$ resulting from phonon-assisted optical absorption using the maximally localized Wannier function method to interpolate the quasiparticle energies, velocity matrix elements, phonon frequencies, and electron-phonon-coupling matrix elements onto fine BZ-sampling grids needed to converge the spectra. The fine electronic k -point and phonon q -point sampling grids we employed are $32 \times 32 \times 32$ for 3C, $24 \times 24 \times 16$ for 2H, $24 \times 24 \times 12$ for 4H, $24 \times 24 \times 8$ for 6H, and $24 \times 24 \times 24$ for 15R. The delta function in Eq. (1) is approximated by a Gaussian function with a broadening of 0.05 eV to resolve fine features close to the absorption edge.

The direct part of the optical spectra is calculated including electron-hole Coulomb interactions by solving the Bethe-Salpeter equation for the optical polarization function, implemented in the BERKELEYGW package [41,42,50]. The electron-hole interaction kernel is calculated on the homogeneous electronic k grid as in the GW calculations and interpolated to the following finer grid through considering the wave function overlap between the fine grids and coarse grids [42]. A small arbitrary shift is applied to all of the fine grids to ensure smooth spectra: $12 \times 12 \times 12$ for 3C, $8 \times 8 \times 6$ for 2H, $8 \times 8 \times 3$ for 4H, $9 \times 9 \times 3$ for 6H, and $8 \times 8 \times 8$ for 15R. For the direct part of the spectra, a Gaussian function with a broadening of 0.15 eV is used to model the delta function. The imaginary part of the dielectric function is calculated for a total number of bands of two times the number of valence bands for each polytype (corresponding to a maximum energy of at least 30 eV and ~ 15 eV above valence band maximum) and the real part of the dielectric function is evaluated by summing the direct and phonon-assisted part of $\epsilon_2(\omega)$ and utilizing the Kramers-Kronig relationship. The combined real and imaginary parts of the dielectric function are then used to evaluate the refractive indices (n_r) and absorption coefficients (see Appendix A 1 for the comparison between the calculated n_r and experimental measurements). We mention that the imaginary part of the dielectric function resulting from the phonon-assisted process is typically a few orders of magnitude smaller than that resulting from direct transitions. As a result, the contribution of the phonon-assisted process to the overall integral in the Kramers-Kronig relationship is usually negligible, i.e., the difference between the refractive index obtained with and without considering the phonon-assisted contribution is small.

In addition to the approach derived above from second-order perturbation theory, phonon-assisted optical properties can be obtained by properly displacing the atoms in supercells according to the eigenvalues and eigenmodes of the dynamical matrix and calculating direct transitions in the resulting distorted supercells, namely the special displacement method (SDM) [33–35]. The benefit of the SDM approach is that the phonon-induced band gap renormalization, as well as the temperature dependence of the band structure, are taken into consideration by nature with the construction of the specific supercell. With the supercell generated using the SDM, the indirect part of the optical spectra can be directly calculated out using standard approaches utilizing first-order Fermi's golden rule. In our work, we adopted the SDM approach to construct $3 \times 3 \times 3$, $4 \times 4 \times 4$, and $6 \times 6 \times 6$ supercells for the 3C polytype to compare the SDM approach with the standard approach. We note that, in the SDM approach, due to the requirement of calculations for large supercells, evaluating electron-hole interactions via the BSE formalism becomes computationally expensive; thus our optical calculation is limited to the independent-particle picture.

III. RESULT AND DISCUSSION

A. Structural, electronic, and phonon properties

The calculated structural parameters for all polytypes considered in this study are listed in Table I and are in good

TABLE I. Lattice constants (in Å) of the investigated SiC polytypes as calculated in the present study and compared to previous theoretical and experimental studies. For the 3C structure, the lattice parameters are also converted to the equivalent 3H structure and shown in parentheses. Our calculated values are in excellent agreement with experimental data for all polytypes with a maximum difference of 0.8%.

Polymorph	Space group	This work		Previous theory		Experiment	
		a	c	a	c	a	c
3C (3H)	$F\bar{4}3m$ (206)	4.382 (3.099)		4.372 (3.091) [51]		4.358 (3.082) [2]	
2H	$P6_3mc$ (186)	3.094	5.077	3.086 [51]	5.065 [51]	3.076 [2]	5.048 [2]
4H	$P6_3mc$ (186)	3.096	10.135	3.094 [51]	10.129 [51]	3.073 [2]	10.053 [2]
6H	$P6_3mc$ (186)	3.097	15.194	3.094 [51]	15.185 [51]	3.081 [2]	15.117 [2]
15R	$R3m$ (160)	3.090	37.910	3.082 [52]	37.796 [52]	3.07–3.08 [53]	37.30–37.80 [53]

agreement with previously reported computational results and experimental measurements. Our results for the lattice constants of all polytypes agree well with literature values using the same type of exchange-correlation functional (PBE), with the maximum difference not exceeding 0.3%. For better comparison to the hexagonal polytypes, we convert the cubic lattice parameter of the 3C structure to the equivalent hexagonal 3H structure [2], i.e., $a_{3H} = \frac{1}{\sqrt{2}}a_{3C}$, which is shown in the parentheses in Table I. For hexagonal structures, our calculations show a minor expansion of the a lattice constant and a contraction of the c lattice constant as the number of hexagonal layers increases. Their variation, however, is on the order of the variation of the experimental lattice constant reported by different authors [2,54–56]. Overall, the theoretical lattice constants are consistently overestimated in comparison to experiment, which is expected for the GGA type of exchange-correlation functionals due to its known underbinding of chemical bonds. However, the calculated trend of the variation of lattice parameters across different polytypes agrees well with experimental measurements. The maximum overestimation of the calculated lattice constant compared to the experimental value is only 0.8%.

The electronic band structures of all investigated polytypes of SiC are shown in Fig. 1. From the figure it can be clearly seen that all polytypes exhibit indirect band gaps that are much smaller than their direct band gaps. Overall, we see that the band structure of the 3C structures shows clearly the smallest indirect band gap and the largest direct gap compared to other polytypes. It is interesting to notice that the 2H structure exhibits a different feature than the other hexagonal structures (4H and 6H): whereas the conduction band minimum (CBM) of 4H and 6H SiC occurs at the M point of the BZ, the CBM of 2H SiC occurs at the K point, while the local minimum at M lies about 0.4 eV higher in energy. Later, we show that this difference between the 2H structure and the other hexagonal polytypes induce a unique double bumplike feature in its indirect optical absorption as described in Sec. III C.

We next show that our calculated electronic band gaps agree well both with experiment and with previous calculations for all SiC polytypes. The calculated band gaps of the different SiC polytypes are listed in Table II. The PBE results exhibit the well-known underestimation of the band gap for all polytypes. However, including quasiparticle corrections with the GW approximation, the calculated band gap is in much better agreement with experimental measurements, with the differences being within 0.15 eV. Our results exhibit a consistent trend as other theoretical and experimental studies:

the indirect gap of the material decreases as the number of hexagonal layers increase. Meanwhile, the 3C structure shows a band gap about 1 eV narrower than all other polytypes, while the 15R structures show slightly smaller band gap compared to the 6H structure. It can be seen, however, that our calculated GW band gap does not consistently overestimate or underestimate the experimental gap. The difference between our GW result in comparison to other literature values may result from the plasmon-pole model, the different starting point due to the exchange-correlation functional, etc. The difference between the calculated value from the GW approximation and the experimentally measured value is attributed in part to the lack of temperature-related renormalization (~ 0.03 – 0.05 eV [22]) of the band gap and the zero-point motion. Nevertheless, the differences between our calculated GW band gap and experimental measurements are in general within 0.15 eV, with the 3C structure being the largest but not exceeding 7%. We note that fine-tuning the electronic-structure methodology to obtain a better match of the gap to experiment is not the focus of this work; thus we restrict our band-structure calculation to the one-shot GW approximation.

We further show the calculated phonon band structures and we show that the phonon frequencies agree well with both experimental measurements as well as theoretical studies. The calculated phonon band structures for all different SiC polytypes are shown in Fig. 2. The maximum phonon frequency at Γ is very similar across all different polytypes, with a variation within the range from 117.0 meV to 117.2 meV. Compared to available experimental data (see marks for the data and references in Fig. 2), the differences are less than 3%. We also compared the calculated phonon frequencies to first-principles results [69] using ABINIT [70] and the differences of the calculated phonon frequencies are no larger than 2%. The calculated electron phonon matrix elements are interpolated onto a fine \mathbf{q} and \mathbf{k} grid utilizing Wannier interpolation to obtain converged phonon-assisted optical spectra that we show later in Sec. III C.

B. Direct optical properties

We first report the calculated direct part of the absorption spectra and the dielectric constants, with excitonic effects included. The optical spectra shown in Fig. 3 (ordinary direction for the hexagonal structures) are calculated with quasiparticle energies from the GW approximation and with electron-hole interaction from the BSE approach. Our calculated optical spectra agree well with literature [71] for the 3C, 2H, and

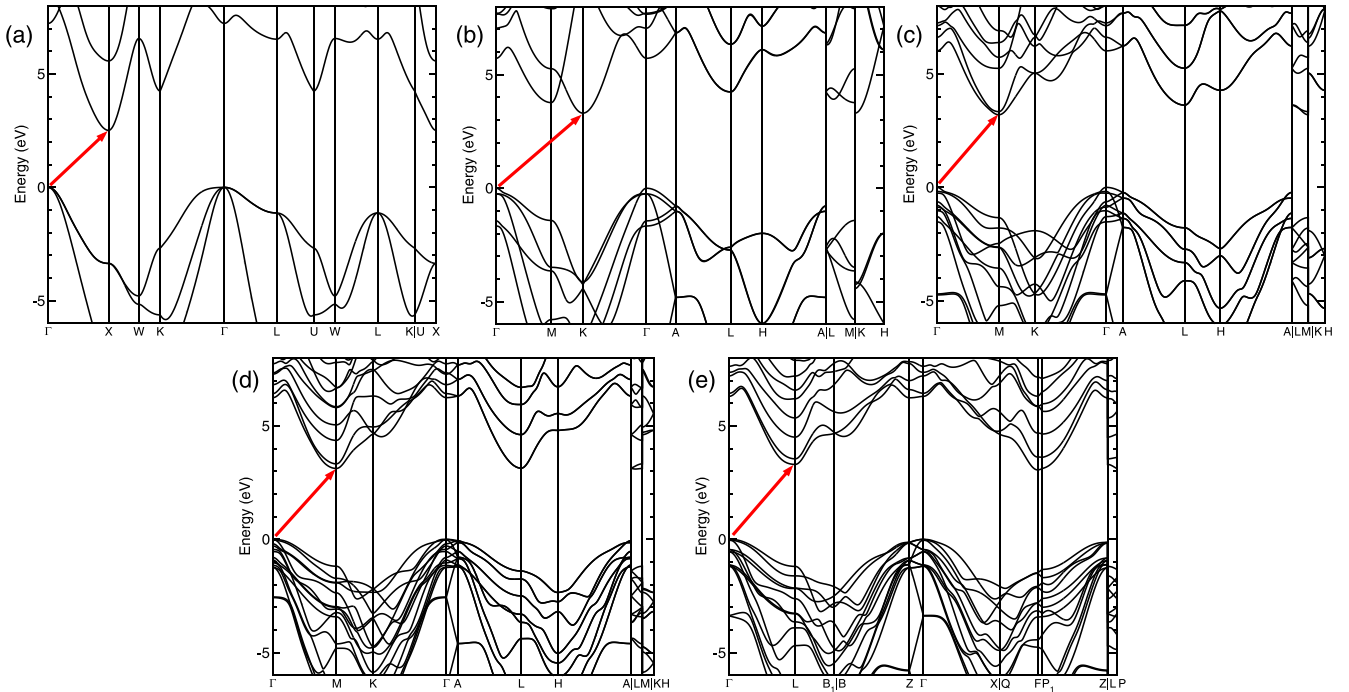


FIG. 1. Quasiparticle band structures of the five investigated SiC polytypes: (a) 3C, (b) 2H, (c) 4H, (d) 6H, and (e) 15R, calculated with the *GW* method and interpolated with the maximally localized Wannier function method. All polytypes are indirect-gap semiconductors (the indirect gap is marked with red arrows).

6H structure, especially considering the relative height and position of the main peak. Similar to Ref. [71] we observe a significant shoulder close to the absorption onset (~ 6 eV) that is clearest for 3C SiC, while being less significant for 2H and 6H. It is worthwhile to note that our spectra are noticeably higher than in Ref. [71], which is due to the different choice of broadening parameters used to approximate the delta function (0.15 eV in this work versus 0.25 eV in the reference). We report the calculated dielectric constants in Table III. Our calculated dielectric constants are higher than Ref. [71] and this can be affected by many factors, including possible different BSE energy cutoffs and different quasiparticle band gaps, etc. Overall, the maximum difference between our calculated dielectric constant and experimental values is 6.3%. Since in the indirect part of the spectra, the imaginary part of the dielectric functions are orders of magnitudes smaller than the direct part, it is reasonable to assume that the refractive index is approximately proportional to the square root of the real part of the dielectric function. As a result, in this case

the difference in the calculated direct spectra from theory to experiment does not affect the calculated indirect part of the spectra by a maximum of 3%. Later in this section, we show that this is a minor effect compared to other factors, for example, the finite-temperature band-gap renormalization or the mere difference of the band gap from *GW* approximation to experiment.

C. Phonon-assisted optical properties from second-order perturbation theory

Following the calculation of the direct spectra, we determine the phonon-assisted indirect optical spectra of the SiC polytypes, evaluated with the second-order time-dependent perturbation theory. We find that our results agree well with experiments for the most common polytypes (3C, 4H, and 6H) and we can predict the indirect spectra for 2H and 15R polytypes. Figure 4 shows the calculated absorption coefficient in the region of indirect absorption for all polytypes. Additional rigid shifts Δ are applied to the quasiparticle

TABLE II. Calculated band gaps (in eV) of the five investigated SiC polytypes both within PBE and with the *GW* approximation, in comparison to previous theoretical and experimental results. Our data are in good agreement with previous work with a maximum difference of 0.15 eV.

Polytype	This work, PBE	Previous theory, GGA	This work, <i>GW</i>	Previous theory, <i>GW</i>	Experiment
3C	1.373	1.391 [51], 1.410 [57]	2.514	2.38 [58], 2.24 [59], 2.59 [60]	2.360 [61]
2H	2.335	2.350 [57]	3.311	3.33 [58]	3.330 [62]
4H	2.244	2.238 [57]	3.205	3.26 [58], 3.11 [59]	3.230 [61]
6H	2.050	2.034 [51], 2.031 [57]	3.127	3.05 [58]	3.000 [61]
15R	1.977	2.16 [63]	3.062		2.986 [64]

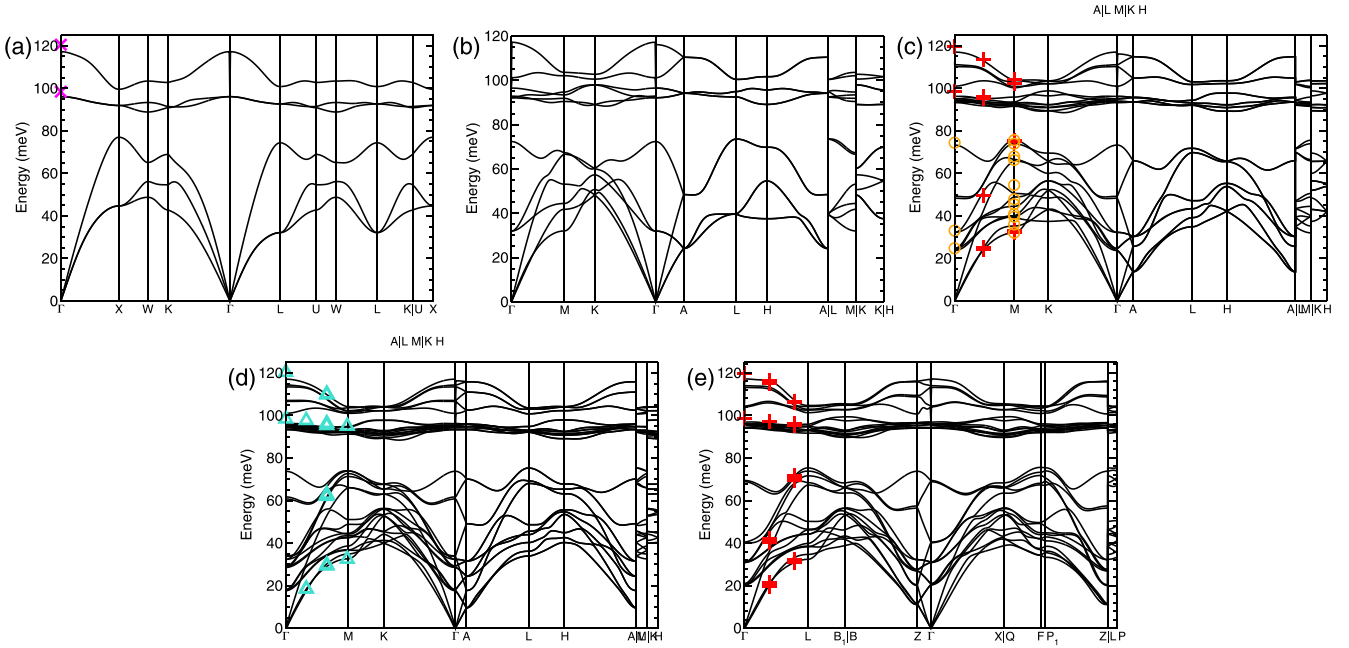


FIG. 2. Calculated phonon dispersions of the investigated SiC polytypes (a) 3C, (b) 2H, (c) 4H, (d) 6H, and (e) 15R. Our calculated phonon frequencies underestimate available experimental measurements by less than 3%. Experimental data are plotted from Ref. [65] (3C, purple crosses), Ref. [66] (4H and 15R, red plus), Ref. [67] (4H, orange circles), and Ref. [68] (6H, blue upper triangles). Compared to previous theoretical studies [69], we find very good agreement of the dispersion compared to experiment, with maximum differences of the phonon frequencies on the order of 2%.

energies from the *GW* approximation to match the indirect gap from experiment: $\Delta = -0.154$ eV for 3C, $\Delta = 0.019$ eV for 2H, $\Delta = 0.025$ eV for 4H, $\Delta = -0.126$ eV for 6H, and $\Delta = -0.076$ eV for 15R. For completeness, we show the original unshifted spectra in Appendix A 4. For the indirect part of the spectra, it is reasonable to assume that the correction on the band gap can be well represented with a rigid shift of the absorption coefficient (i.e., no scaling of the spectra is needed) [33]. We compared the calculated absorption coefficient in the indirect region of the 3C, 4H, and 6H polytypes to experimental measurements and we find a good agreement with the experimental results. For the 15R structure, we observe that the absorption coefficient in the indirect region is similar to the 6H structure. Such similarity is expected due to the similarities in the electronic band structure and phonon band structures. Interestingly, for the 2H structure, we observe

TABLE III. Dielectric constant for the ordinary polarization ($\epsilon_{\infty}^{\perp}$) calculated with the BSE approach for the five SiC polytypes. Our calculated dielectric constants overestimate experimental values by a maximum of 6.3% (3C), resulting in less than 3% overestimation for the refractive index.

Polytype	This work, BSE	Theory, BSE (Ref. [71])	Experiment (Ref. [72])
3C	6.93	6.36	6.52
2H	6.89	6.27	6.51
4H	6.84		
6H	6.79	6.31	6.52
15R	6.73		

two bumplike features around photon energies of 3.45 eV and 3.75 eV. We note that these two energies correspond to the energy difference between the valence band maximum at Γ and the conduction band minimum at K , as well as the second minimum at M , respectively. The closeness of the energies and the momentums of these two valleys leads to the two bumplike features. This is a unique feature that we only observe in the 2H structure; as for all other hexagonal structures, a second distinct valley close to the CBM in both energy and momentum is not observed.

Stepping forward, our first-principles tools allow us to investigate the temperature dependency of the indirect optical properties to examine the factors that affect the spectra as temperature changes. As a thermally stable material, many of the novel optoelectronic applications of SiC involve extreme conditions [76–78]. Therefore, being able to predict temperature-dependent optical properties from a first-principles perspective can provide crucial information for novel applications. We calculated the temperature-dependent indirect optical spectra for the 4H and 6H polytypes at three different temperatures (300 K, 473 K, and 573 K). The calculated temperature-dependent absorption coefficients in the indirect region are shown in Fig. 5. Additional rigid shifts are applied to match the calculated electronic band gap with experimentally determined values [61]. It can be seen from the figure that our calculation reproduces the relative change in the indirect optical absorption due to temperature changes very well after taking the band gap renormalization into account (see Appendix A 2 for spectra without additional rigid shift). We conclude that the effects of temperature on both the phonon occupation numbers as well as on the renormalization of the band gap itself are important to obtain

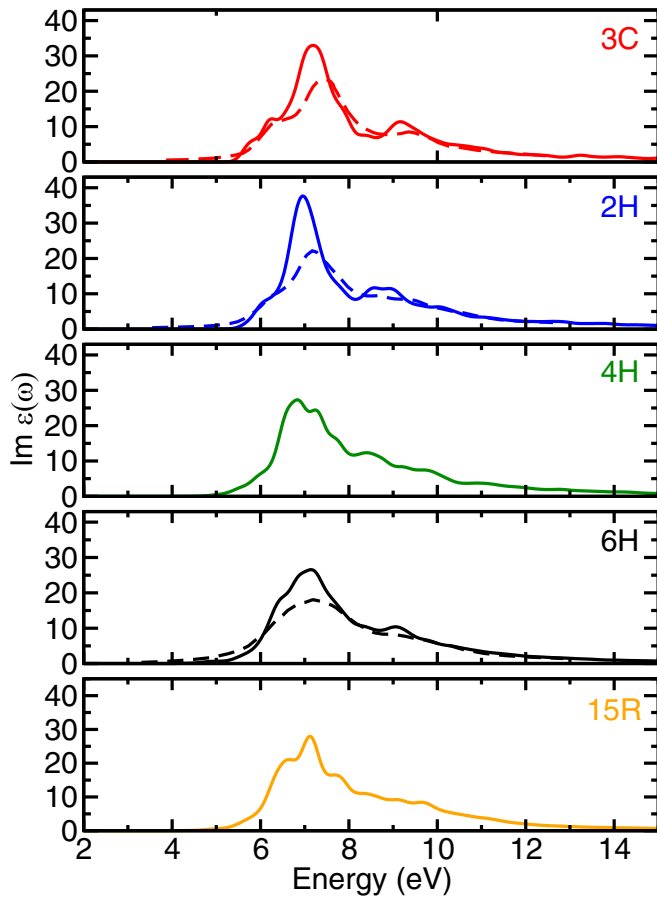


FIG. 3. Solid: calculated direct part of the optical absorption spectra (imaginary part of the complex dielectric function) for the ordinary light polarization for the five different SiC polytypes, including quasiparticle effects with the *GW* approximation and electron-hole interactions via the BSE equation. Dashed: theoretical BSE data from Ref. [71] for 3C, 2H, and 6H polytypes. We find very good agreement in terms of the peak positions and shapes, with the height of the peak potentially affected by the choice of the broadening parameters.

reliable prediction of the indirect absorption spectra. However, for the 6H polytype, we find that the simple rigid shift of the gap does not accurately provide the correct positions of the shoulder of the absorption curve. In the next section, we examine an alternative route to calculate phonon-assisted absorption that avoids the rigid-shift approach and considers implicitly the temperature renormalization of the band structure.

D. Phonon-assisted optical properties from the special displacement method (SDM)

Next, we show that the effect of temperature-related renormalizations of the band gap on the optical absorption spectra of SiC can be overcome by applying the special displacement method. Although the SDM approach only requires a single snapshot of the atomic displacement configuration [33–35], the need to perform calculations on relatively large supercells (approaching thousands of atoms) results in a drastic increase in the computational cost. As a result, we take quasiparticle

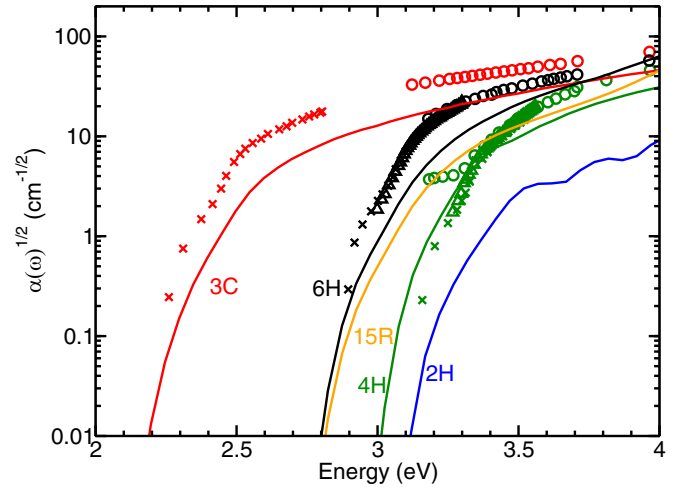


FIG. 4. Calculated optical absorption coefficient for the ordinary direction ($E \perp c$) at 300 K for the five investigated SiC polytypes in the phonon-assisted spectral region between the indirect and direct band gaps. The experimental results from the literature are taken from Ref. [73] (3C, 4H, and 6H, cross mark), Ref. [74] (4H and 6H, circle marks), and Ref. [75] (4H and 6H, upper triangle mark). A rigid shift has been applied to each theoretical curve to correct the difference between the *GW*-calculated gaps and the experimental values at 300 K listed in Table II for each polytype. The calculated absorption spectra are in overall good agreement with experiment.

corrections into account using a rigid increase of the gap (1.141 eV) to account for the difference between the PBE band gap and the *GW* band gap from unit cell calculations. In Fig. 6, we show the best converged results using the SDM approach compared to the perturbation approach for 3C SiC. The same rigid shift is applied for the perturbation approach as indicated in the previous sections. In the SDM approach, no artificial shifts are applied except for the indirect-band-gap correction from the PBE to the *GW* value. At energies beyond 3 eV, the SDM approach shows better agreement quantitatively compared to the experimental data. This is because, by taking the renormalization of the band gap with respect to temperature into account, the SDM approach is more physical in terms of predicting the correct position of the absorption peaks. However, below a photon energy of 3 eV, the perturbation approach predicts the shape of the curve better. There are a few possible factors. First, it is straightforward to use the perturbation approach utilizing Wannier interpolation to obtain matrix elements on the fine grid, which is important in order to obtain converged spectra near the absorption onset that require a fine sampling of the Brillouin zone. For the SDM approach, however, convergence with respect to supercell size is required. In our work, we find that underconverged supercell can incur significant error for the absorption onset, or incorrect absorption shoulders, and a $6 \times 6 \times 6$ supercell is needed for converged phonon-assisted spectra (see Appendix A 3). Second, the nature of the approach corresponds to neglecting the explicit phonon frequencies in the δ function of calculating $\varepsilon_2(\omega)$ in Eq. (1); thus the absorption onset can be affected [33–35].

Overall, we show that, although both the SDM approach and the perturbation approach provide satisfying

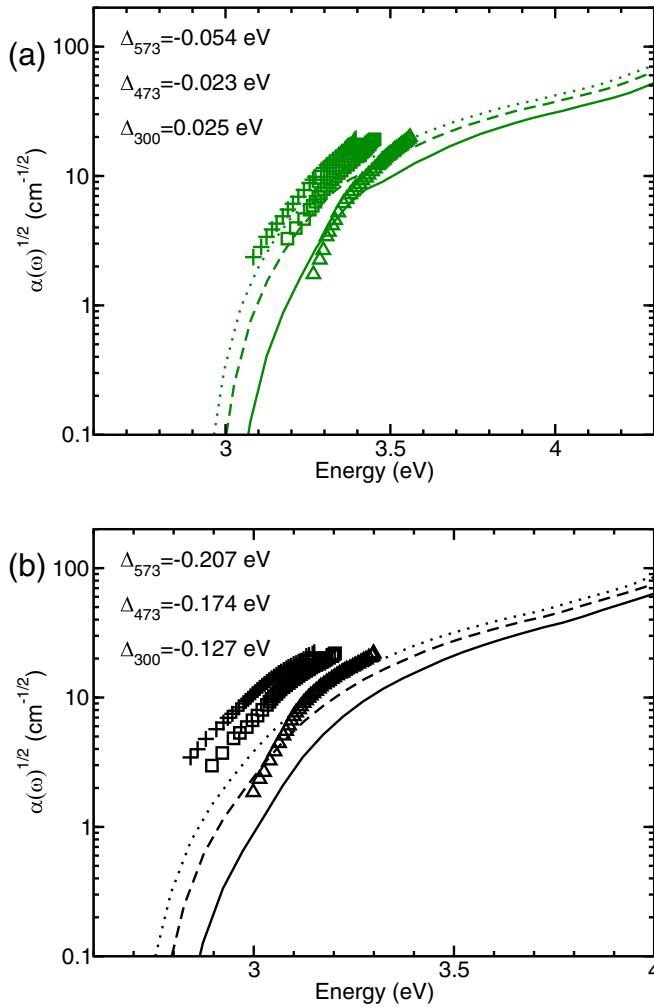


FIG. 5. Calculated absorption coefficient for (a) 4H SiC and (b) 6H SiC as a function of photon energy in the phonon-assisted region (lines) for a temperature of 300 K (solid), 473 K (dashed), and 573 K (dotted), and compared to experimental measurements (data points) from Ref. [75] at 300 K (upper triangle), 473 K (square), and 573 K (plus). The theoretical curves have been rigidly shifted to match the temperature dependence of the experimental band gap according to Ref. [61]. The change in the spectra with respect to temperature change is well predicted with the changes in band gaps included.

results for predicting the phonon-assisted optical absorption properties for 3C SiC, the SDM approach clearly illustrates the importance of including the correct temperature-dependent renormalization of the band gap to obtain higher quantitative accuracy. The special displacement approach also shows the potential of further investigations, e.g., excitonic effects on the indirect part of the optical spectra by performing BSE calculations on properly converged supercells. However, fully converged BSE calculations on such large supercells are computationally challenging and beyond the scope of this paper. Meanwhile, it is also clear that, to resolve the finer structures of the optical absorption around the absorption edge, it is important to fully consider the effects of phonons including the phonon energies.

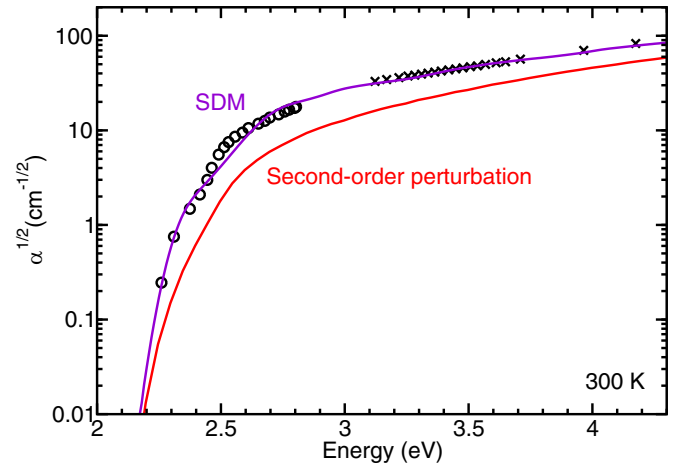


FIG. 6. Calculated absorption coefficient as a function of energy for the 3C polytype with $6 \times 6 \times 6$ supercell with the special displacement (SDM) approach [35] using a $4 \times 4 \times 4$ \mathbf{k} -points grid (violet) and the perturbation approach (red solid) ($32 \times 32 \times 32$ \mathbf{k}/\mathbf{q} -points grid). Experimental data from Ref. [73] (black circles) and Ref. [74] (black cross) are shown for comparison. The same rigid shift is applied as in Fig. 4 for the perturbation approach, while no rigid shift is applied for the SDM approach. The renormalization of the band gap due to temperature is physically included with the SDM approach.

IV. CONCLUSION

In this work, we investigate the phonon-assisted optical properties of five different SiC polytypes with first-principles calculations. We first calculate the structural properties of all polytypes with density functional theory, and electronic properties with the *GW* approximation, and we show that the calculated results agree well with both other theoretical studies and experimental measurements. We then utilize Wannier interpolation to obtain the electron-phonon coupling in dense electronic and phonon grids and we use second-order time-dependent perturbation theory to obtain phonon-assisted optical spectra in the indirect gap region of all polytypes. We show that the simulated absorption coefficient in the indirect region agrees well with experimental measurements for the most common 3C, 4H, and 6H polytypes and provides prediction for 15R and 2H polytypes. Further analysis on the temperature-dependent indirect optical properties shows that our theoretical simulation predicts the trend of the variation in optical properties with respect to temperature well and we show that our simulations can be particularly useful in understanding the practical application of the material at various finite temperatures. However, our results show that the renormalization of the band gaps due to temperature is important in predicting the temperature-dependent spectra. Therefore, we further compare the conventional approach utilizing second-order perturbation theory to the method employing special displacement of specific atoms in supercells and we show that improvement of the predictions of the temperature dependency of the indirect optical spectra can be obtained by taking the renormalization of the electronic energies implicitly due to temperature change into account. Our work shows that these methods enable quantitative predictions of temperature-

dependent phonon-assisted absorption spectra in indirect-gap semiconductor materials.

ACKNOWLEDGMENTS

We thank Dr. M. Zacharias for the fruitful discussion about the SDM approach. The work is supported as part of the Computational Materials Sciences Program funded by the U.S. Department of Energy, Office of Science, Basic Energy Sciences, under Award No. DE-SC0020129. Computational resources were provided by the National Energy Research Scientific Computing Center, which is supported by the Office of Science of the U.S. Department of Energy under Contract No. DE-AC02-05CH11231.

APPENDIX: SUPPLEMENTAL DATA

1. Refractive index

In this section we show the calculated refractive index compared to experimental measurements. Figure 7 shows that our calculated refractive index of 3C, 4H, and 6H polytypes agrees very well with experimental measurements, with the difference being an overestimation by less than 3%. These differences in the refractive index from our calculation compared to experiments are a negligible source of error even compared to the mere difference of the band gaps themselves.

2. Temperature-dependent indirect spectra

In this section, we demonstrate the temperature-dependent indirect spectra without including the additional rigid shifts to account for the temperature-dependent band-gap renormalization. In Fig. 8, we show the calculated optical spectra without considering the difference between calculated band gap and experimentally measured band gap. It can be seen clearly that, first, the effects of temperature on the indirect optical spectra itself are still clear and this is mainly due to the change in the Bose-Einstein occupation factor of the phonons. However,

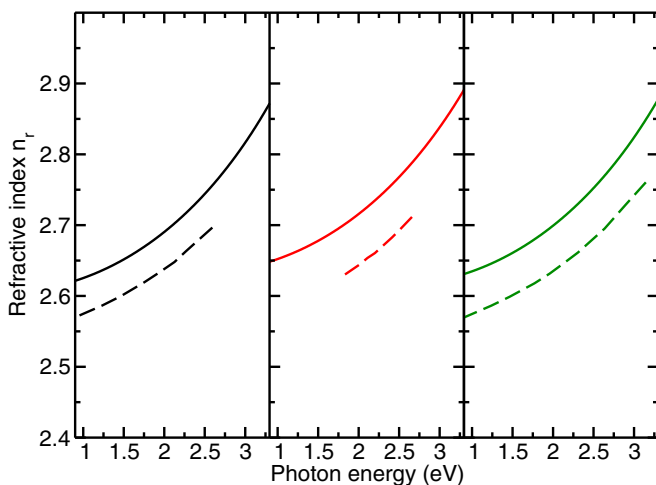


FIG. 7. Calculated refractive index in the region close to the indirect band gap for 4H SiC (black solid), 3C SiC (red solid), and 6H SiC (green solid), as well as comparison to experimental curve (dashed) from Ref. [79] (4H and 6H) and Ref. [80] (3C).

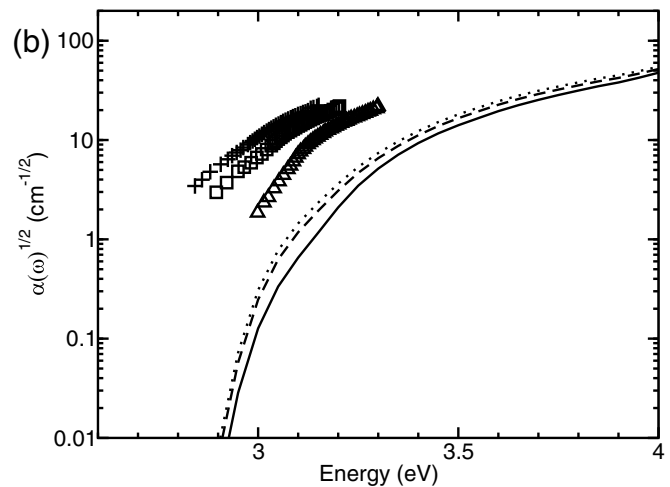
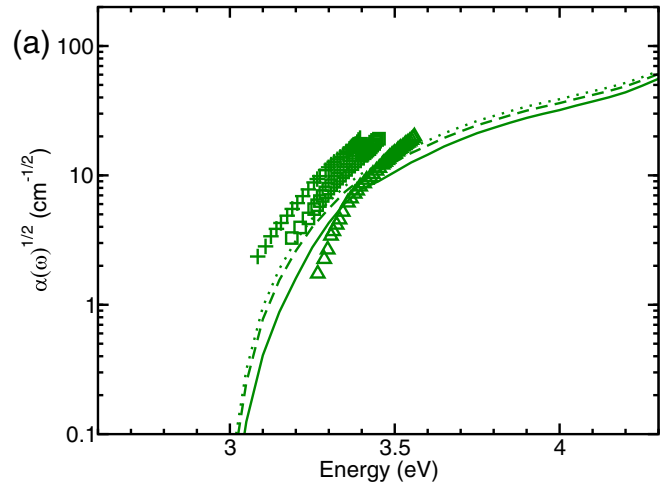


FIG. 8. Calculated absorption coefficient for 4H SiC (a) and 6H SiC (b) as a function of photon energy in the indirect region (lines) for a temperature of 300 K (solid), 473 K (dashed), and 573 K (dotted), and compared to experimental measurements (data points) from Ref. [75] at 300 K (upper triangle), 473 K (square), and 573 K (plus). The difference with Fig. 5 is the omission of the correction to the band-gap value to match experiment.

without considering the difference in band gap from theory and from experiment, especially in the 6H case, the onset of absorption is severely overestimated and, more importantly in this context, the differences between the curves at different temperatures are underestimated. This clearly shows the importance of considering both the change in occupations due to temperature and the changes in band gap itself due to temperature change, as the change in spectra is clearly a combined effect of both.

3. Convergence of the supercell approach

To test the convergence of the supercell approach versus the supercell size, we calculated the indirect optical spectra with $3 \times 3 \times 3$, $4 \times 4 \times 4$, and $6 \times 6 \times 6$ supercells. In this section we report the convergence behavior of the calculated spectra near the absorption onset in Fig. 9. It can be seen from the figure that the two smaller supercells are not sufficient

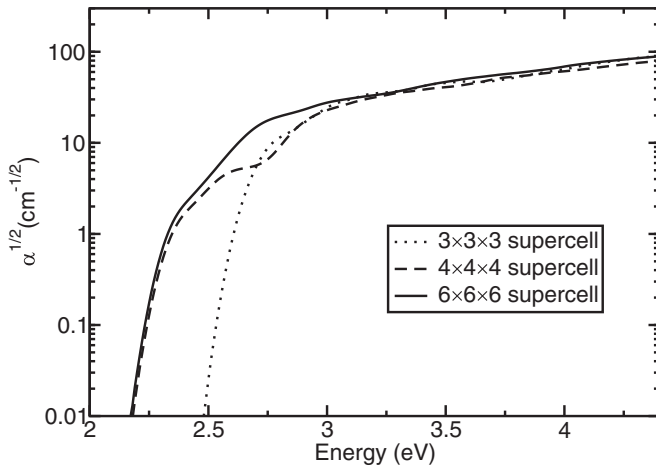


FIG. 9. Calculated absorption coefficient using the special displacement approach [35] with three different supercell sizes: $3 \times 3 \times 3$ (dotted), $4 \times 4 \times 4$ (dashed), and $6 \times 6 \times 6$ (solid). The \mathbf{k} -points sampling are $8 \times 8 \times 8$, $6 \times 6 \times 6$, and $4 \times 4 \times 4$, respectively. All k -point grids are randomly shifted for better convergence. Convergence beyond $6 \times 6 \times 6$ cell requires supercells with more than 1000 atoms and is not tested due to the large computational cost.

for converged optical spectra in the indirect region. The best converged results of the $6 \times 6 \times 6$ supercell are reported in the main text.

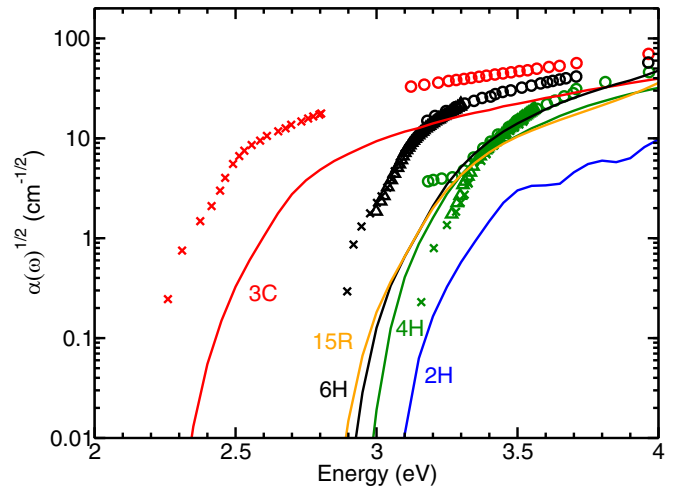


FIG. 10. Calculated absorption coefficient of the different SiC polytypes without rigid shift as described for Fig. 4.

4. Indirect absorption coefficient without rigid shift

In this section, we show the absorption coefficient calculated from our first-principle data without any rigid shift to match the experimentally measured band gap. It can be clearly seen from Fig. 10 that the differences in the predicted band gap and experimentally measured band gap need to be taken into consideration in order to achieve good agreement.

- [1] F. R. Chien, S. R. Nutt, W. S. Yoo, T. Kimoto, and H. Matsunami, Terrace growth and polytype development in epitaxial β -SiC films on α -SiC (6H and 15R) substrates, *J. Mater. Res.* **9**, 940 (1994).
- [2] Z. C. Feng, *SiC Power Materials: Devices and Applications* (Springer Science & Business Media, New York, 2013), Vol. 73.
- [3] A. Yaghoubi, R. Singh, and P. Melinon, Predicting the primitive form of rhombohedral silicon carbide (9R-SiC): A pathway toward polytypic heterojunctions, *Cryst. Growth Des.* **18**, 7059 (2018).
- [4] J. Edmond, H. Kong, A. Suvorov, D. Waltz, and C. Carter, Jr, 6H-silicon carbide light emitting diodes and UV photodiodes, *Phys. Status Solidi A* **162**, 481 (1997).
- [5] D. M. Brown, E. Downey, J. Kretchmer, G. Michon, E. Shu, and D. Schneider, SiC flame sensors for gas turbine control systems, *Solid State Electron.* **42**, 755 (1998).
- [6] S. Przybylko, Developments in silicon carbide for aircraft propulsion system applications, in *29th Joint Propulsion Conference and Exhibit* (American Institute of Aeronautics and Astronautics, Monterey, CA 1993), p. 2581.
- [7] H. Aida, T. Doi, H. Takeda, H. Katakura, S.-W. Kim, K. Koyama, T. Yamazaki, and M. Uneda, Ultraprecision CMP for sapphire, GaN, and SiC for advanced optoelectronics materials, *Curr. Appl. Phys.* **12**, S41 (2012).
- [8] H. Okumura, Present status and future prospect of widegap semiconductor high-power devices, *Jpn. J. Appl. Phys.* **45**, 7565 (2006).
- [9] T. Kimoto, K. Fujihira, H. Shiomi, and H. Matsunami, High-voltage 4H-SiC schottky barrier diodes fabricated on (0338) with closed micropipes, *Jpn. J. Appl. Phys.* **42**, L13 (2003).
- [10] W. Gao, F. Zhang, Z. Zheng, and J. Li, Unique and tunable photodetecting performance for two-dimensional layered MoSe₂/WSe₂ p-n junction on the 4H-SiC substrate, *ACS Appl. Mater. Interfaces* **11**, 19277 (2019).
- [11] Y. Liu, Y. Xu, B. Cao, Z. Li, E. Zhao, S. Yang, C. Wang, J. Wang, and K. Xu, Transferable GaN films on Graphene/SiC by van der Waals epitaxy for flexible devices, *Phys. Status Solidi A* **216**, 1801027 (2019).
- [12] M.-Q. Li, N. Yang, G.-G. Wang, H.-Y. Zhang, and J.-C. Han, Highly preferred orientation of Ga₂O₃ films sputtered on SiC substrates for deep UV photodetector application, *Appl. Surf. Sci.* **471**, 694 (2019).
- [13] C. Huang, H. Zhang, and H. Sun, Ultraviolet optoelectronic devices based on AlGaIn-SiC platform: Towards monolithic photonics integration system, *Nano Energy* **77**, 105149 (2020).
- [14] M. Kim, J.-H. Seo, U. Singiseti, and Z. Ma, Recent advances in free-standing single crystalline wide band-gap semiconductors and their applications: GaN, SiC, ZnO, β -Ga₂O₃, and diamond, *J. Mater. Chem. C* **5**, 8338 (2017).
- [15] H. Mousa, M. A. Yildirim, and K. Teker, Performance enhancement of 3C-SiC thin film UV photodetector via gold nanoparticles, *Semicond. Sci. Technol.* **34**, 095002 (2019).
- [16] H. Ahmed, A. Hashim, and H. Abduljalil, Determination of optical parameters of films of PVA/TiO₂/SiC and PVA/MgO/SiC

- nanocomposites for optoelectronics and UV-detectors, *Ukr. J. Phys.* **65**, 533 (2020).
- [17] J. Bradford, M. Shafiei, J. MacLeod, and N. Motta, Synthesis and characterization of WS₂/graphene/SiC van der Waals heterostructures via WO_{3-x} thin film sulfuration, *Sci. Rep.* **10**, 17334 (2020).
- [18] E. Scalise, A. Marzegalli, F. Montalenti, and L. Miglio, Temperature-Dependent Stability of Polytypes and Stacking Faults in SiC: Reconciling Theory and Experiments, *Phys. Rev. Appl.* **12**, 021002(R) (2019).
- [19] R. Schomer, P. Friedrichs, D. Peters, and D. Stephani, Significantly improved performance of MOSFETs on silicon carbide using the 15R-SiC polytype, *IEEE Electron Device Lett.* **20**, 241 (1999).
- [20] S. Mourya, J. Jaiswal, G. Malik, B. Kumar, and R. Chandra, Structural and optical characteristics of in-situ sputtered highly oriented 15R-SiC thin films on different substrates, *J. Appl. Phys.* **123**, 023109 (2018).
- [21] H. Yano, T. Kimoto, H. Matsunami, M. Bassler, and G. Pensl, MOSFET performance of 4H-, 6H-, and 15R-SiC processed by dry and wet oxidation, in *Materials Science Forum* (Trans Tech Publications Ltd., Zurich-Uetikon, Switzerland, 2000), Vol. 338, pp. 1109–1112.
- [22] W. J. Choyke, Optical properties of polytypes of SiC: Interband absorption, and luminescence of nitrogen-exciton complexes, in *Silicon Carbide-1968* (Elsevier, Amsterdam, 1969), pp. S141–S152.
- [23] J. R. O'Connor and J. Smiltens, *Silicon Carbide, a High Temperature Semiconductor: Proceedings of the Conference on Silicon Carbide* (Pergamon Press, New York, 1960).
- [24] W.-H. Zhang, F.-C. Zhang, W.-B. Zhang, S.-L. Zhang, and W. Yang, First-principle study of the structural, electronic, and optical properties of SiC nanowires, *Chin. Phys. B* **26**, 057103 (2017).
- [25] S. Majidi, S. M. Elahi, A. Esmailian, and F. Kanjouri, First principle study of electronic and optical properties of planar GeC, SnC and SiC nanosheets, *Prot. Met. Phys. Chem. Surf.* **53**, 773 (2017).
- [26] C. Xie, P. Xu, F. Xu, H. Pan, and Y. Li, First-principles studies of the electronic and optical properties of 6H-SiC, *Phys. B: Condens. Matter* **336**, 284 (2003).
- [27] K.-H. Lee, C. Park, B.-H. Cheong, and K.-J. Chang, First-principles study of the optical properties of SiC, *Solid State Commun.* **92**, 869 (1994).
- [28] Y. Niu, H. Hu, W. Zhang, J. Li, L. Qiao, N. Dong, and P. Han, First-principle study of electronic structure and optical properties of SiC nano films, *Semicond. Sci. Technol.* **34**, 115015 (2019).
- [29] J. Song, Y. Yang, and H. Liu, Electronic structures and optical properties of nitrogen-doped SiC nanotube, in *2009 IEEE International Conference of Electron Devices and Solid-State Circuits (EDSSC)* (IEEE, New York, 2009), pp. 509–512.
- [30] Z. Xu, Y. Li, and Z. Liu, Controlling electronic and optical properties of layered SiC and GeC sheets by strain engineering, *Mater. Des.* **108**, 333 (2016).
- [31] N. Marzari, A. A. Mostofi, J. R. Yates, I. Souza, and D. Vanderbilt, Maximally localized Wannier functions: Theory and applications, *Rev. Mod. Phys.* **84**, 1419 (2012).
- [32] F. Giustino, Electron-phonon interactions from first principles, *Rev. Mod. Phys.* **89**, 015003 (2017).
- [33] M. Zacharias and F. Giustino, One-shot calculation of temperature-dependent optical spectra and phonon-induced band-gap renormalization, *Phys. Rev. B* **94**, 075125 (2016).
- [34] M. Zacharias, C. E. Patrick, and F. Giustino, Stochastic Approach to Phonon-Assisted Optical Absorption, *Phys. Rev. Lett.* **115**, 177401 (2015).
- [35] M. Zacharias and F. Giustino, Theory of the special displacement method for electronic structure calculations at finite temperature, *Phys. Rev. Res.* **2**, 013357 (2020).
- [36] P. Giannozzi, S. Baroni, N. Bonini, M. Calandra, R. Car, C. Cavazzoni, D. Ceresoli, G. L. Chiarotti, M. Cococcioni, I. Dabo *et al.*, QUANTUM ESPRESSO: A modular and open-source software project for quantum simulations of materials, *J. Phys.: Condens. Matter* **21**, 395502 (2009).
- [37] P. Giannozzi, O. Andreussi, T. Brumme, O. Bunau, M. B. Nardelli, M. Calandra, R. Car, C. Cavazzoni, D. Ceresoli, M. Cococcioni *et al.*, Advanced capabilities for materials modelling with Quantum ESPRESSO, *J. Phys.: Condens. Matter* **29**, 465901 (2017).
- [38] J. P. Perdew, K. Burke, and M. Ernzerhof, Generalized Gradient Approximation Made Simple, *Phys. Rev. Lett.* **77**, 3865 (1996).
- [39] D. R. Hamann, Optimized norm-conserving Vanderbilt pseudopotentials, *Phys. Rev. B* **88**, 085117 (2013).
- [40] M. Schlipf and F. Gygi, Optimization algorithm for the generation of ONCV pseudopotentials, *Comput. Phys. Commun.* **196**, 36 (2015).
- [41] M. S. Hybertsen and S. G. Louie, Electron correlation in semiconductors and insulators: Band gaps and quasiparticle energies, *Phys. Rev. B* **34**, 5390 (1986).
- [42] J. Deslippe, G. Samsonidze, D. A. Strubbe, M. Jain, M. L. Cohen, and S. G. Louie, BerkeleyGW: A massively parallel computer package for the calculation of the quasiparticle and optical properties of materials and nanostructures, *Comput. Phys. Commun.* **183**, 1269 (2012).
- [43] J. Deslippe, G. Samsonidze, M. Jain, M. L. Cohen, and S. G. Louie, Coulomb-hole summations and energies for GW calculations with limited number of empty orbitals: A modified static remainder approach, *Phys. Rev. B* **87**, 165124 (2013).
- [44] S. Baroni, S. de Gironcoli, A. Dal Corso, and P. Giannozzi, Phonons and related crystal properties from density-functional perturbation theory, *Rev. Mod. Phys.* **73**, 515 (2001).
- [45] F. Giustino, M. L. Cohen, and S. G. Louie, Electron-phonon interaction using Wannier functions, *Phys. Rev. B* **76**, 165108 (2007).
- [46] S. Poncé, E. Margine, C. Verdi, and F. Giustino, EPW: Electron-phonon coupling, transport and superconducting properties using maximally localized Wannier functions, *Comput. Phys. Commun.* **209**, 116 (2016).
- [47] C. Verdi and F. Giustino, Fröhlich Electron-Phonon Vertex from First Principles, *Phys. Rev. Lett.* **115**, 176401 (2015).
- [48] J. Noffsinger, E. Kioupakis, C. G. Van de Walle, S. G. Louie, and M. L. Cohen, Phonon-Assisted Optical Absorption in Silicon from First Principles, *Phys. Rev. Lett.* **108**, 167402 (2012).
- [49] X. Zhang, G. Shi, J. A. Leveillee, F. Giustino, and E. Kioupakis, *Ab initio* theory of free-carrier absorption in semiconductors, *Phys. Rev. B* **106**, 205203 (2022).
- [50] M. Rohlfing and S. G. Louie, Electron-hole excitations and optical spectra from first principles, *Phys. Rev. B* **62**, 4927 (2000).

- [51] N. D. Alkhalidi, S. K. Barman, and M. N. Huda, Crystal structures and the electronic properties of silicon-rich silicon carbide materials by first principle calculations, *Heliyon* **5**, e02908 (2019).
- [52] W. Ching, Y.-N. Xu, P. Rulis, and L. Ouyang, The electronic structure and spectroscopic properties of 3C, 2H, 4H, 6H, 15R and 21R polymorphs of SiC, *Mater. Sci. Eng. A* **422**, 147 (2006).
- [53] K. Järrendahl and R. F. Davis, Materials properties and characterization of SiC, in *Semiconductors and Semimetals* (Elsevier, Amsterdam, 1998), Vol. 52, pp. 1–20.
- [54] C. H. Park, B.-H. Cheong, K.-H. Lee, and K. J. Chang, Structural and electronic properties of cubic, 2H, 4H, and 6H SiC, *Phys. Rev. B* **49**, 4485 (1994).
- [55] M. Stockmeier, R. Müller, S. A. Sakwe, P. J. Wellmann, and A. Magerl, On the lattice parameters of silicon carbide, *J. Appl. Phys.* **105**, 033511 (2009).
- [56] O. Madelung, *Semiconductors: Group IV Elements and III-V Compounds* (Springer Science & Business Media, New York, 2012).
- [57] Z. Huang, T.-Y. Lü, H.-Q. Wang, and J.-C. Zheng, Thermoelectric properties of the 3C, 2H, 4H, and 6H polytypes of the wide-band-gap semiconductors SiC, GaN, and ZnO, *AIP Adv.* **5**, 097204 (2015).
- [58] V. N. Brudnyi and A. V. Kosobutsky, Electronic structure and the local electroneutrality level of SiC polytypes from quasiparticle calculations within the GW approximation, *J. Exp. Theor. Phys.* **114**, 1037 (2012).
- [59] G. L. Zhao and D. Bagayoko, Electronic structure and charge transfer in 3C- and 4H-SiC, *New J. Phys.* **2**, 16 (2000).
- [60] B. Wenzien, P. Käckell, F. Bechstedt, and G. Cappellini, Quasiparticle band structure of silicon carbide polytypes, *Phys. Rev. B* **52**, 10897 (1995).
- [61] M. E. Levinshstein, S. L. Rumyantsev, and M. S. Shur, *Properties of Advanced Semiconductor Materials: GaN, AlN, InN, BN, SiC, SiGe* (John Wiley & Sons, New York, 2001).
- [62] L. Patrick, D. Hamilton, and W. Choyke, Growth, luminescence, selection rules, and lattice sums of SiC with wurtzite structure, *Phys. Rev.* **143**, 526 (1966).
- [63] F. C. Zhang, Y. Gao, H. W. Cui, X. X. Ruan, and W. H. Zhang, First-principles study on electronic structure of 15R-SiC polytypes, in *Advanced Materials Research* (Trans Tech Publ, 2014), Vol. 971, pp. 77–80.
- [64] R. Humphreys, D. Bimberg, and W. Choyke, Wavelength modulated absorption in SiC, *Solid State Commun.* **39**, 163 (1981).
- [65] H. Nienhaus, T. Kampen, and W. Mönch, Phonons in 3C-, 4H-, and 6H-SiC, *Surf. Sci.* **324**, L328 (1995).
- [66] D. W. Feldman, J. H. Parker, W. J. Choyke, and L. Patrick, Phonon dispersion curves by Raman scattering in SiC, polytypes 3C, 4H, 6H, 15R, and 21R, *Phys. Rev.* **173**, 787 (1968).
- [67] S. Bai, Y. Ke, Y. Shishkin, O. Shigiltchhoff, R. P. Devaty, W. J. Choyke, D. Strauch, B. Stojetz, B. Dorner, D. Hobgood *et al.*, Four current examples of characterization of silicon carbide, *MRS Online Proc. Libr.* **742**, 31 (2002).
- [68] D. W. Feldman, J. H. Parker, W. J. Choyke, and L. Patrick, Raman scattering in 6H SiC, *Phys. Rev.* **170**, 698 (1968).
- [69] G. Petretto, S. Dwaraknath, H. P. Miranda, D. Winston, M. Giantomassi, M. J. Van Setten, X. Gonze, K. A. Persson, G. Hautier, and G.-M. Rignanese, High-throughput density-functional perturbation theory phonons for inorganic materials, *Sci. Data* **5**, 180065 (2018).
- [70] X. Gonze, J.-M. Beuken, R. Caracas, F. Detraux, M. Fuchs, G.-M. Rignanese, L. Sindic, M. Verstraete, G. Zerah, F. Jollet, M. Torrent, A. Roy, M. Mikami, P. Ghosez, J.-Y. Raty, and D. Allan, First-principles computation of material properties: The ABINIT software project, *Comput. Mater. Sci.* **25**, 478 (2002).
- [71] M. Rohlfiing and J. Pollmann, Dielectric function and reflectivity spectrum of SiC polytypes, *Phys. Rev. B* **63**, 125201 (2001).
- [72] G. L. Harris, *Properties of Silicon Carbide* (IET, London, UK 1995), Vol. 13.
- [73] P. Ščajev, M. Kato, and K. Jarašiūnas, A diffraction-based technique for determination of interband absorption coefficients in bulk 3C-, 4H- and 6H-SiC crystals, *J. Phys. D: Appl. Phys.* **44**, 365402 (2011).
- [74] S. G. Sridhara, T. J. Eperjesi, R. P. Devaty, and W. J. Choyke, Penetration depths in the ultraviolet for 4H, 6H and 3C silicon carbide at seven common laser pumping wavelengths, *Mater. Sci. Eng. B* **61**, 229 (1999).
- [75] N. Watanabe, T. Kimoto, and J. Suda, Temperature dependence of optical absorption coefficient of 4H- and 6H-SiC from room temperature to 300, *Jpn. J. Appl. Phys.* **53**, 108003 (2014).
- [76] A. Lohrmann, B. C. Johnson, J. C. McCallum, and S. Castelletto, A review on single photon sources in silicon carbide, *Rep. Prog. Phys.* **80**, 034502 (2017).
- [77] M. V. Kazakova, V. A. Karachinov, I. G. Djerenov, and D. A. Evstigneev, Analysis of reflected radiation from a semitransparent mirror of silicon carbide, *IOP Conf. Ser.: Mater. Sci. Eng.* **441**, 012023 (2018).
- [78] M. Ebrahimi, A. A. Schmidt, C. Kaplan, O. Schmitz, and P. Czermak, Innovative optical-sensing technology for the online fouling characterization of silicon carbide membranes during the treatment of oily water, *Sensors* **20**, 1161 (2020).
- [79] S. Wang, M. Zhan, G. Wang, H. Xuan, W. Zhang, C. Liu, C. Xu, Y. Liu, Z. Wei, and X. Chen, 4H-SiC: A new nonlinear material for midinfrared lasers, *Laser Photon. Rev.* **7**, 831 (2013).
- [80] P. T. B. Shaffer, Refractive index, dispersion, and birefringence of silicon carbide polytypes, *Appl. Opt.* **10**, 1034 (1971).